Crystallographic Analyses of NADH Peroxidase Cys42Ala and Cys42Ser Mutants: Active Site Structures, Mechanistic Implications, and an Unusual Environment of Arg 303[†,‡]

Sharmila S. Mande,[§] Derek Parsonage,[||] Al Claiborne,[||] and Wim G. J. Hol*[,§]

Department of Biological Structure, Biomolecular Structure Program and Howard Hughes Medical Institute SL-15, School of Medicine, University of Washington, Seattle, Washington 98195, and Department of Biochemistry, Wake Forest University Medical Center, Winston-Salem, North Carolina 27157

Received January 11, 1995; Revised Manuscript Received April 4, 1995[⊗]

ABSTRACT: NADH peroxidase from *Enterococcus faecalis* is a tetrameric flavoenzyme of 201 400 Da which employs Cys 42 as a redox-active center cycling between sulfhydryl (Cys-SH) and sulfenic acid (Cys-SOH) states along the catalytic pathway. The role of the active site cysteine 42 in NADH peroxidase has been elucidated using biochemical and crystallographic techniques. Here we describe the crystal structures of two active site cysteine mutants, Cys42Ala and Cys42Ser, which were determined to 2.0 Å resolution and refined to crystallographic *R* values of 17.6 and 18.3%, respectively. The overall chain fold and the quaternary structure of the two mutants appear to be very similar to wild-type enzyme. Therefore, the substantially lower activity of the mutants is due to the absence of the Cys-SOH redox center. One of the oxygen atoms of the nonnative cysteine sulfonic acid in the wild-type structure is replaced by a water molecule in both mutant structures. Two other residues near the active site are His 10 and Arg 303. A detailed analysis of the environment of these residues in the mutant and wild-type peroxidase structures indicates that the imidazole ring of His 10 is uncharged. The interactions made by the guanidinium group of Arg 303 involve not only His 10 but also the carboxylate of Glu 14 and Tyr 60. Interestingly, the $N^{\eta 1}H$ function of Arg 303 is oriented perpendicular to the plane of the phenyl ring of Tyr 60 with a $N^{\eta 1}$ to phenyl ring center distance of 3.8 Å, suggesting a favorable electrostatic interaction between Arg 303 and Tyr 60. This indicates that Tyr 60 might play a role in the precise positioning of Arg 303. In its turn the positive charge of Arg 303 next to the imidazole ring of His 10 suggests that the latter residue remains unprotonated throughout the catalytic cycle.

The NADH peroxidase from *Enterococcus faecalis* 10C1 (Claiborne *et al.*, 1992, 1993, 1994) is unique among flavoproteins in its ability to catalyze the direct reduction of $H_2O_2 \rightarrow 2H_2O$. In these heme-deficient, strictly fermentative, facultative anaerobes the enzyme plays dual roles in the defense against peroxide-mediated oxidative stress and in regenerating NAD^+ as required for glycolysis. Although the peroxidase exhibits a number of structural and mechanistic similarities to the flavoprotein disulfide reductases [e.g., lipoamide dehydrogenase (Williams, 1992)], its utilization of a cysteine-sulfenic acid (Cys-SOH) redox center (Poole & Claiborne, 1989a) instead of a redox-active cystine disulfide represents a primary point of distinction between the peroxide and disulfide reductases. Flavin-mediated reduction of the Cys42-SOH center by NADH generates the anionic thiolate form of Cys42-SH, which serves as the nucleophile against the electrophilic H_2O_2 substrate. In this regard Cys42-SH of the reduced peroxidase exhibits functional similarities to the selenol (Cys-SeH) form of the selenoenzyme glutathione peroxidase (Flohé *et al.*, 1972; Epp *et al.*, 1983) and to cysteine proteases such as papain (Kamphuis *et al.*, 1984). However, the reversible oxidation/reduction of Cys 42 in NADH peroxidase between the SH and SOH states is distinctly different from the role of the catalytic cysteine in sulfhydryl proteases. The reversible oxidation of Cys 42 in NADH peroxidase is obviously very similar to that of the selenocysteine residue in glutathione peroxidase.

On the basis of kinetic and structural information, a general reaction mechanism has been proposed for the NADH peroxidase (Claiborne *et al.*, 1993) which is as follows. First the peroxidase is reduced by NADH in an initial priming step:

$$E(SOH) + NADH + H^+ \rightarrow EH_2(SH) + NAD^+ + H_2O$$

In the steady state the enzyme cycles between EH_2 and EH_2·NADH forms:

$$EH_2(SH) + NADH \rightarrow EH_2(SH)\cdot NADH$$

$$EH_2(SH)\cdot NADH + H_2O_2 \rightarrow E(SOH)\cdot NADH + H_2O$$

$$E(SOH)\cdot NADH \rightarrow EH_2(SH) + NAD^+ + H_2O$$

The mode of NADH binding to the oxidized peroxidase has also been determined through crystallographic analysis of the E(Cys42-SO_3H)−NADH complex (Stehle *et al.*,

[†] A grant from the Murdock Charitable Trust to the Biomolecular Structure Program at the University of Washington School of Medicine is gratefully acknowledged (W.G.J.H). A.C. acknowledges support from the National Institutes of Health (NIH), Grant GM-35394.

[‡]Coordinates have been deposited in the Brookhaven Protein Data Bank under the file names 1NHP and 1NHQ.

* To whom correspondence should be addressed.

[§] University of Washington, Seattle.

[||] Wake Forest University Medical Center.

[⊗] Abstract published in *Advance ACS Abstracts,* May 15, 1995.

0006-2960/95/0434-6985$09.00/0

1993). This established that the nicotinamide ring is situated at the other side (*re* face) of the FAD isoalloxazine ring, the distance between the S^{γ} of Cys42 and the C4 of the nicotinamide being 6.9 Å. A detailed reaction mechanism has been proposed by Stehle *et al.* (1993). In addition to the redox active Cys 42 and FAD, His 10 is proposed to participate in the reaction through both electrostatic (as protonated His 10) and hydrogen bonding interactions with reaction intermediates.

The NADH peroxidase sequence (Ross & Claiborne, 1991) exhibits limited homology to the sequences of lipoamide dehydrogenase and glutathione reductase, but the refined 2.16 Å crystal structure of the wild-type enzyme (Stehle *et al.*, 1991) reveals a domain organization very similar to these disulfide reductases (Mattevi *et al.*, 1992, 1993; Karplus & Schulz, 1987). The active-site Cys 42 is found within the N-terminal FAD-binding domain; unfortunately the Cys42-SOH center is oxidized to the nonnative Cys42-SO_3H (cysteine-sulfonic acid) in the wild-type enzyme structure determined crystallographically. One oxygen atom (OX1) of Cys42-SO_3H is hydrogen bonded to both His10-$N^{\epsilon 2}$ and to Cys42-N, and the suggestion has been made (Stehle *et al.*, 1993) that OX1 closely approximates the position of the original Cys42-SOH oxygen. In NADH peroxidase His 10 is located near Arg 303, an interaction which is entirely different from the structurally equivalent histidine residue in lipoamide dehydrogenase and glutathione reductase (Benen *et al.*, 1991; Rietveld *et al.*, 1994). In the latter enzymes an ion pair is formed between the histidine and a glutamate, conserved in lipoamide dehydrogenase and glutathione reductase (Benen *et al.*, 1991; Rietveld *et al.*, 1994). This glutamate is absent in the peroxidase. Hence the environment of the active-site His 10 is distinctly different in the disulfide oxidoreductases and NADH peroxidase and will be the subject of detailed analysis in the present paper.

Given the refractile behavior of the reduced peroxidase Cys42-SH toward chemical modification (Poole & Claiborne, 1989b), active-site mutants in which this residue is replaced by Ala and Ser have been expressed and characterized in detail (Parsonage & Claiborne, 1995) in order to unravel the importance of this residue for catalysis. In agreement with the proposed key function of Cys 42, as expected, the absence of the redox-active Cys42 renders these proteins virtually devoid of peroxidatic activity (0.04% residual activity), although the respective rates of flavin reduction by NADH are rapid. More surprisingly, the flavin redox potentials for the mutants are increased by approximately 100 mV over that of the two-electron-reduced (EH_2) wild-type enzyme. Since the Ser for Cys substitution is essentially isosteric and since Ser 42 cannot be oxidized during X-ray analysis, these mutants also provide the opportunity for gaining additional insights into the active-site structure of the reduced (Cys42-SH) wild-type enzyme. In this report we present the refined structures of the NADH peroxidase Cys42Ala and Cys42Ser mutants and analyze the environments of active site residues Cys/Ala/Ser 42, His 10, and Arg 303.

MATERIALS AND METHODS

The expression and purification of the NADH peroxidase Cys42Ala and Cys42Ser mutants has been described in detail (Parsonage & Claiborne, 1995). The purified proteins, at concentrations of 4−14 mg/mL in 50 mM potassium phosphate, pH 6.8, containing 0.6 mM EDTA, formed the starting point for the crystallization experiments.

Table 1: Summary of Crystal Parameters and Data Collection

	C42A	C42S	wild type[a]
space group	*I*222	*I*222	*I*222
cell dimensions (Å)			
a	77.6	77.6	77.2
b	134.8	135.1	134.5
c	146.3	146.5	145.9
V_M (Å^3 per dalton)	3.80	3.82	3.76
number of subunits per asymmetric unit	1	1	1
wavelength (Å)	1.54	0.91	0.96
resolution (Å)	2.0	2.0	2.16
completeness of data (%)			
cumulative	90.6	94.1	92.0
last shell (2.09−2.04 Å)	74.2	96.3	*b*
unique reflections used	49 100	48 245	37 857
merging *R* factor (%)[c]	4.2	9.4	10.6

[a] From Stehle *et al.* (1991). [b] Not available. [c] Merging *R* factor = $\sum |I - \langle I \rangle| / \sum \langle I \rangle$.

Crystallization and Data Collection. Crystals were obtained by the vapor diffusion technique at room temperature. The protein solution contained 7 and 3 mg/mL of the C42A and C42S mutants, respectively, in 25 mM potassium phosphate buffer at pH 7.0 with 0.3 mM EDTA and 2 mM dithiothreitol. The reservoir contained 1.9 M ammonium sulfate, 5 μM FAD, and 100 mM potassium phosphate buffer, pH 7.0. A hanging drop of 10 μL was prepared by mixing 5 μL amounts of protein and reservoir solutions. Both mutants crystallized isomorphously with wild-type NADH peroxidase in the orthorhombic space group *I*222 (Stehle *et al.*, 1991). Data for the C42A mutant were collected at room temperature using an X100 Siemens area detector mounted on a RIGAKU (RU200) rotating anode operated at 40 kV and 70 mA, equipped with a graphite monochromator. The crystal-to-detector distance was kept at 100 mm. An oscillation range of 0.15° per frame was used. Crystal parameters and data collection statistics are given in Table 1. Data processing, reduction, merging, and scaling were accomplished using the program XENGEN (Howard *et al.*, 1987). After the final scaling the R_{sym} for 49 100 reflections was 0.042 for the C42A mutant. The crystals of the C42S mutant diffracted to only 3.0 Å on the area detector; 2.0 Å data of the C42S mutant up to 2.0 Å could, however, be collected on the CHESS F1 beam line with a crystal-to-image plate distance of 200 mm and a crystal oscillation range of 2.0° per exposure. These data were processed using MOSFLM (Leslie *et al.*, 1991) and scaled using the ROTAVATA and AGROVATA programs of the CCP4 suite (CCP4, 1994). The overall R_{merge} up to 2.0 Å for this C42S data set of 48 245 unique reflections is 0.094.

Refinement. The starting model used for the refinement of both mutants was the wild-type structure (Stehle *et al.*, 1991). In order to avoid model bias for the side chain of residue 42 in the mutants, the triply oxidized cysteine 42 was converted into glycine by deleting the C^{β}, S^{γ}, and the three oxygen atoms of the oxidized cysteine from the atomic coordinates. The starting *R* factors at this stage were 33.9 and 41.0% for the C42A and C42S mutants, respectively. Crystallographic refinement of positions and individual *B* factors was carried out by using the conjugate gradient option of the program X-PLOR (Brünger *et al.*, 1987). Only reflections with $F > 2\sigma(F)$ and with Bragg spacing between 8.0 and 2.0 Å were used in the refinement. σ_A weighted maps (Read, 1986) with coefficients $||F_o| - |F_c|| \exp(i\varphi_c)$

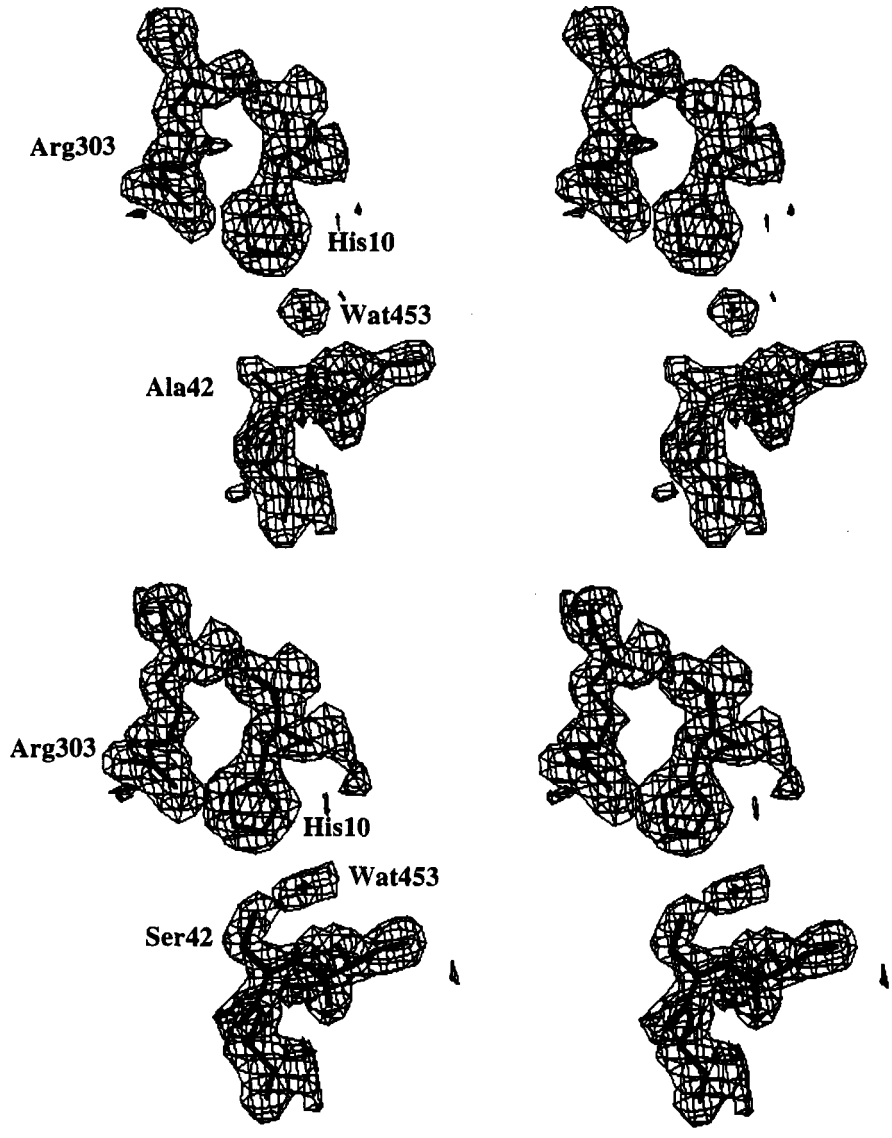

FIGURE 1: Stereoview of a $2|F_o| - |F_c|$ map showing electron density for residue 42, His 10, Arg 303, and the active site water, WAT453 in (a, top) the C42A mutant. The hydrogen bonded distances are as follows: Ala42 N to WAT453, 2.7 Å; WAT453 to His10 $N^{\epsilon 2}$, 2.8 Å; His10 $N^{\delta 1}$ to Arg303 $N^{\eta 1}$, 3.1 Å. (b, bottom) The C42S mutant. The hydrogen bond distances are Ser42 N to WAT453, 2.6 Å; WAT453 to His10 $N^{\epsilon 2}$, 2.9 Å; His10 $N^{\delta 1}$ to Arg303 $N^{\eta 1}$, 3.2 Å.

and $2m|F_o| - D|F_c| \exp(i\varphi_c)$, where $m = \langle\cos(\alpha_o - \alpha_c)\rangle$, $D = \langle\cos(2\pi s\Delta r)\rangle$, and φ_c is the calculated phase from the model were displayed on a Silicon Graphics work station using the program O (Jones *et al.*, 1991). These maps clearly showed the density of the mutated residue 42 corresponding to Ala in the C42A mutant and to Ser in the C42S mutant. Before further refinement, residue 42 was then changed to Ala and Ser in the two mutants. Electron density corresponding to residue 42 is shown in Figure 1. Water molecules were identified by searching peaks above 3 standard deviations from the mean in a ($|F_o| - |F_c|$) map by the program PEKPIK from the XTAL package (Hall & Stewart, 1987). It was ensured that the distance of these peaks from the nearest protein atom was not less than 2.5 Å and not more than 3.5 Å. Before accepting them in the model, they were inspected on an interactive graphics system to check that they formed good hydrogen bonds. Two of the solvent peaks in C42A and one peak in C42S had a tetrahedral appearance. Since the crystals were grown using ammonium sulfate, these peaks were likely to be sulfate ions instead of waters. They were, however, not yet included in the model at this stage of the refinement in which all water molecules were assigned arbitrary initial B factors of 30 Å^2. After carrying out several additional cycles of positional and B factor refinement, the $|F_o| - |F_c|$ map clearly showed three strong peaks, 4σ above the mean electron density at the above-mentioned putative sulfate positions. All three peaks were subsequently treated as sulfate ions. The second sulfate in the C42A mutant was refined with half occupancy. After a total of 280 conjugate gradient cycles, the refinement converged at R factors of 17.6 and 18.3%, respectively, for the C42A and C42S mutants. Table 2 gives the refinement results.

RESULTS AND DISCUSSION

Quality of the Structure. The Ramachandran map (Ramachandran & Sasisekharan, 1968) of the mutant structures is very similar to that of the wild-type protein. The main chain dihedrals of residues Lys 123 and Phe 332, which were found to be outside the allowed region in the wild-type structure, also occupy similar deviating positions in the mutant structures. The geometric criteria as incorporated into the program PROCHECK (Laskowski *et al.*, 1993) show that the geometry of the final model is satisfactory. The

Table 2: Refined Model Parameters for Mutant Proteins

	C42A	C42S
number of unique reflections used[a]	46 357	48 029
resolution range (Å)	8.0−2.0	8.0−2.0
rms. deviations in		
bond lengths (Å)	0.011	0.011
bond angles (deg)	2.6	2.6
improper (deg)	1.0	1.0
dihedral (deg)	25.6	25.8
R factor (%)[b]	17.6	18.3
mean *B* value (Å^2)		
main chain	18.7	16.1
side chain	25.0	22.2
water	38.7	41.0
number of water molecules	243	309

[a] Only reflections with $F > 2\sigma(F)$. [b] *R* factor $= \Sigma||F_o| - |F_c||/\Sigma|F_o|$.

rms deviations from ideality in the bond lengths, bond angles, impropers, and dihedrals have values as shown in Table 2.

The average isotropic temperature factors for all main chain atoms are 18.7 and 16.1 Å^2, respectively, for the C42A and C42S mutants. These values are close to the value of 19.5 Å^2 observed in the wild-type structure. The average main chain *B* factors for the four domains of NADH peroxidase [FAD-binding, NAD-binding, central, and interface domains (Stehle *et al.*, 1991)] are, respectively, 19.8, 20.8, 17.4, and 16.3 Å^2 for the C42A mutant and 17.4, 18.3, 14.6, and 13.5 Å^2 for the C42S enzyme. These values differ little per domain, but the rank order regarding domain mobility is the same in both mutants.

Structural Features. The overall tertiary structures of the two mutants are similar to that of the wild-type enzyme. The rms difference between wild type and C42A for all C^α atoms is 0.14 Å and that for wild type and C42S is 0.15 Å. These low rms values also imply that no relative domain motions or rearrangements occurred in the two mutants. Also the tetramer is the same in the mutants and wild-type enzyme. Thus the mutant structures are virtually identical to the wild type.

The prime interest in this paper is residue 42 and its environment. Residue 42 is situated at the beginning of the helix α2 which comprises residues 43−49 (Figure 2). The maximum atomic shift for residue 42 in the C42A mutant with respect to the wild type is 0.07 Å. In the C42S mutant, the maximum atomic shift is 0.35 Å when comparing the position of O^γ of residue 42 versus that of S^γ in wild type. The *B* factor of the C^β atom in C42A is 7.7 Å^2. Similarly, *B* factors of C^β and O^γ atoms in the C42S mutant are 6.5 and 11.2 Å^2. The corresponding values for C^β and S^γ are 11.0 and 15.1 Å^2 in the wild-type enzyme. This indicates that these residues are well defined in all three structures. The side chain torsional parameters for Ser 42 in the C42S mutant and Cys 42 in the wild-type structure are only slightly different with χ^1 angles being −51° and −44° for the two residues. After the superposition of the complete wild-type and mutant subunits, the rms deviations for the superimposed atoms of residue 42 are 0.06 and 0.07 Å in C42A and C42S mutants, with respect to wild type, respectively. These numbers show that the mutations caused very little structural change. Also the thermal parameters are quite similar. Hence, it has been unequivocally established that the loss of activity of the mutants is due to the loss of the essential sulfhydryl group of residue 42 and not due to a conformational change induced by mutating residue 42.

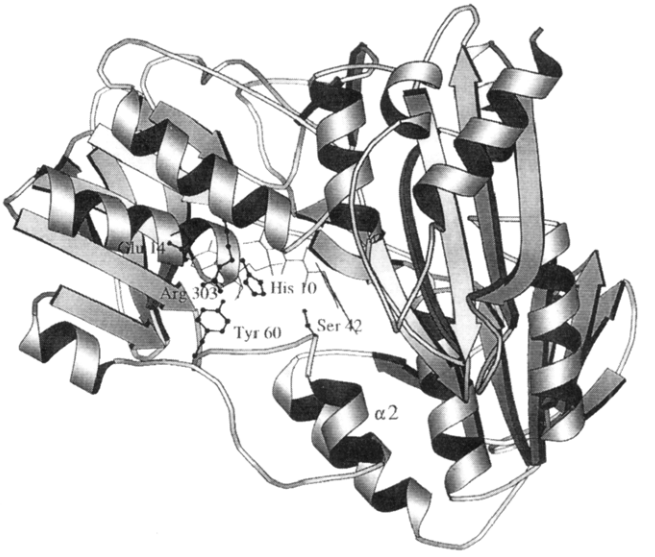

FIGURE 2: Tertiary structure of NADH peroxidase Cys42Ser mutant drawn using MOLSCRIPT (Kraulis, 1991). The site of the mutations, residue 42 (shown with ball and stick), is located at the base of helix α2. The cofactor FAD is drawn with thin lines.

In the wild-type structure the essential Cys42 was triply oxidized. The active site residue, His 10, is located close to residue 42. One of the oxygens, OX1, which linked N of Cys42 and $N^{\epsilon 2}$ of His 10 (Figure 3), has been thought to represent the oxygen of the sulfenic acid (Stehle *et al.*, 1991, 1993). In the present mutants the function of linking residues 42 and 10 is performed by a water molecule, namely, WAT453 (Figure 3 and Table 3). This solvent molecule has low *B* factors of 10.4 and 12.6 Å^2 in the C42A and C42S mutants, respectively. In the C42A mutant, N of Ala42 and $N^{\epsilon 2}$ of His 10 are engaged in hydrogen bonds (with distances of 2.7 and 2.8 Å, respectively) with this active site water. Similarly in the C42S mutant, N and O^γ of Ser 42 and $N^{\epsilon 2}$ of His 10 make hydrogen bonds (with distances of 2.6, 2.7, and 2.9 Å, respectively) with this water molecule. In addition to this hydrogen bond with the active site water, His10 is also involved in a hydrogen bond with Arg 303: the $N^{\delta 1}$ of His 10 to the $N^{\eta 1}$ atom of Arg 303 distances are 3.1 and 3.2 Å in the two mutants. Figure 1 gives a view of the $2F_o - F_c$ maps for the two mutants showing the density of the mutated Cys 42 along with Arg 303, His 10, and the bridging active site water molecule. It is conceivable that this water might be present in the reduced wild-type enzyme for which no structure is available yet. However, when the enzyme is oxidized, this water is displaced in order to make room for the oxygen atom. A similar observation was also made in the crystal structure of dienelactone hydrolase (Pathak *et al.*, 1991) where 60% of the crystal had the active site cysteine in the oxidized state, while the remaining 40% had a water hydrogen bonded to the cysteine sulfhydryl group.

In the wild-type structure, oxygen OX2 of the triply oxidized Cys 42 is centered above the middle ring of the isoalloxazine ring of the FAD, making van der Waals contacts with the C4AF, N5F, C5AF, C9AF, N10F, and C10F atoms of FAD. Due to the removal of oxidized Cys, in the present mutants the OX2 position is not occupied. As a result, a cavity is formed between the isoalloxazine ring of FAD and residue 42. The structural differences near the previous location of the sulfonic acid moiety of the oxidized Cys 42 in the wild type are illustrated in Figure 3. When

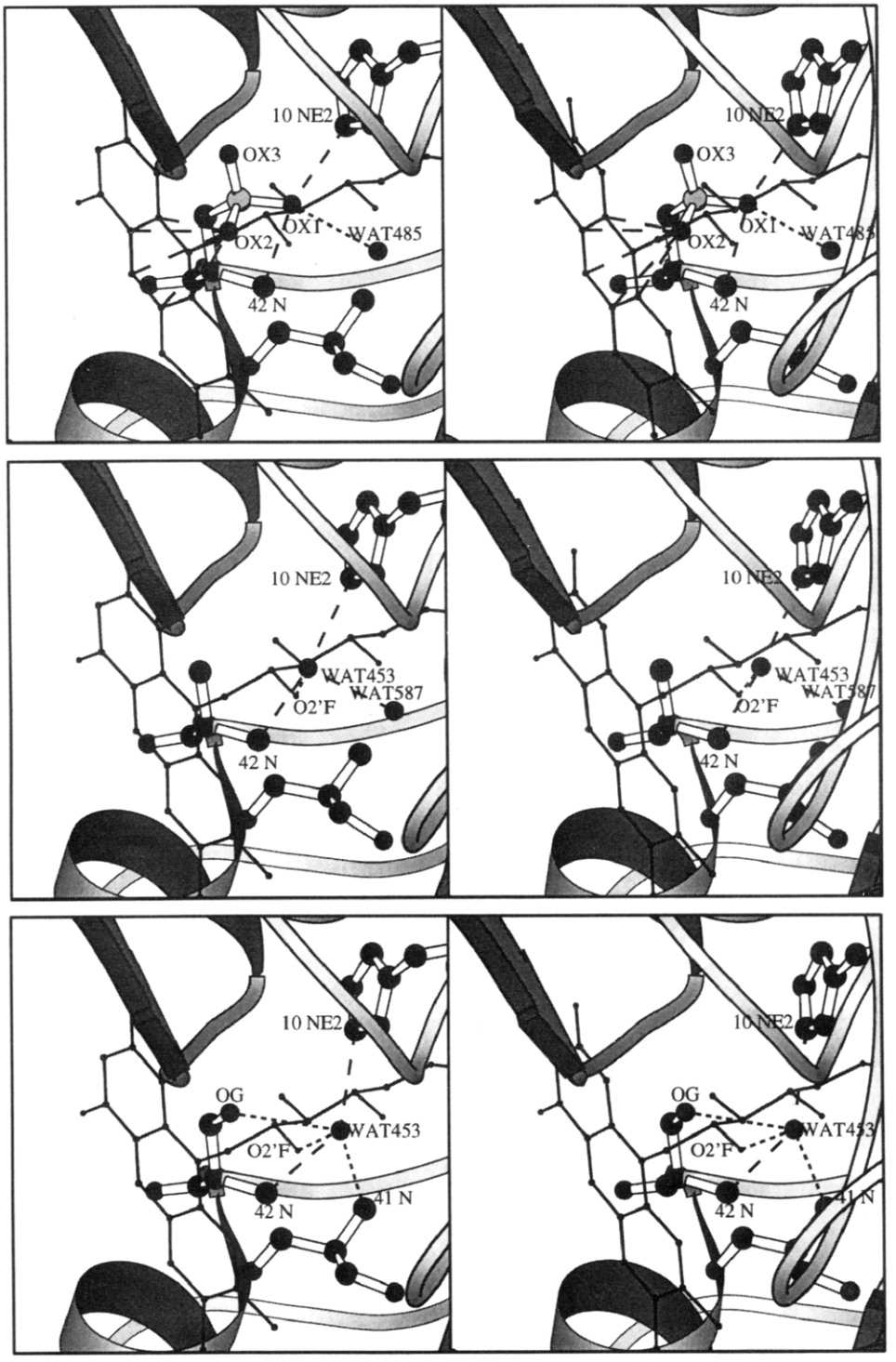

FIGURE 3: Stereoview of a closeup of the structure of NADH peroxidase near residue 42, drawn using the program MOLSCRIPT (Kraulis, 1991). (a, top) Wild type: Cys42 is triply oxidized (OX1, OX2, OX3). OX1 links 42N and His10 $N^{\epsilon 2}$. OX2 makes van der Waals contacts with the isoalloxazine ring of FAD. (b, middle) C42A and (c, bottom) C42S: OX1 is replaced by WAT453. Since the OX2 position is not occupied, a cavity is created between the isoalloxazine ring of FAD and residue 42.

the C^{α} coordinates were superimposed on the native structure, the 18 atoms of the isoalloxazine rings deviate 0.19 and 0.16 Å in the C42A and C42S structures, respectively. This indicates that the alterations near the side chain of residue 42 have virtually no consequences for the position of the flavin ring system in the three molecules.

As explained above, there are changes in the environment of residue 42. Molecular surface areas for residue 42 were calculated using the program CONNOLLY (Connolly, 1983). A probe radius of 1.4 Å was used. The van der Waals surface area for the C^{β} atom of residue 42 is 15.3 and 11.0 $Å^2$ in the two mutants compared to 10.3 $Å^2$ in the wild-type enzyme when the three oxygens of oxidized Cys42 are not included in the calculations. The surface area for O^{γ} in C42S is 4.7 $Å^2$ compared to 6.7 $Å^2$ for S^{γ} in the wild type. Surface calculations were also done after including the active site water in the two mutants and the oxygens of oxidized Cys 42 in the wild type. In the wild-type structure, the surface area for the $N^{\epsilon 2}$ of His10 and S^{γ} of Cys 42 reduces to zero after addition of the three oxygens of the oxidized cysteine. In contrast, although inclusion of WAT453 reduces the surface accessibility of His10 $N^{\epsilon 2}$ to zero in both mutants, Ala42 C^{β} of C42A and Ser42 O^{γ} of C42S retain the same surface area (15.3 and 4.7 $Å^2$, respectively) compared to the

Table 3: Interactions of WAT453[a,b] or Cysteine Sulfonic Acid Oxygens[c] (OX1, OX2, OX3[d]) in the Active Sites of Mutants and Wild-Type NADH Peroxidase

	hydrogen bond partner	distances (Å) in C42A	C42S	wild type
WAT453[a,b]/OX1[c]	42N	2.7	2.6	2.8
	10N$^{\epsilon 2}$	2.8	2.9	2.8
	WAT587[a]/WAT485[c]	2.7		2.8
	FAD O2′F	3.0	3.2	3.5
	42O$^{\gamma}$ [b]		2.7	
	41N	3.5	2.8	3.7
OX2[c]	42N			3.2
	C4AF			2.8
	N5F			2.9
	C5AF			2.9
	C9AF			2.8
	N10F			2.7
	C10F			2.7

[a] In C42A mutant (this work). [b] In C42S mutant (this work). [c] In wild type (Stehle *et al.*, 1991). [d] Atom OX3 is not involved in hydrogen bonds but is accessible to bulk solvent.

Table 4: Interactions of Sulfate Oxygens in the C42A and C42S Mutants of *Enterococcus faecalis* NADH Peroxidase

sulfate ion	sulfate oxygen	hydrogen bond donor	distances (Å) C42A	C42S
449SO_4	O1	159N	3.2	3.2
		160N	3.0	3.0
		WAT494[a]/WAT487[b]	3.0	2.9
	O2	WAT734[b]		3.3
	O3	WAT494[a]/WAT487[b]	2.9	2.9
		WAT620[a]/WAT734[b]	3.1	2.9
		WAT628[a]/WAT639[b]	3.0	2.9
	O4	159N	3.0	3.0
		188OH	2.9	3.0
		WAT628[a]/WAT639[b]	2.7	2.7
450SO_4[c]	O1	WAT562[a]	2.8	
		WAT528[a]	2.9	
		WAT651[a]	2.7	
	O2	WAT490[a]	3.1	
	O3	134N	3.1	
		135N	2.9	
		WAT490[a]	3.0	
		WAT528[a]	2.9	
	O4	134N	3.0	

[a] In C42A mutant. [b] In C42S mutant. [c] This sulfate ion was only observed in C42A mutant.

situation without WAT453. The fact that residue 42 is still accessible in both the mutants is in agreement with the observation that a cavity is present between residue 42 and FAD in both C42A and C42S. Such a cavity, possibly somewhat smaller because of the slightly larger size of a sulfhydryl group compared to a hydroxyl group, might also be present in the wild-type NADH peroxidase.

The solvent structures in both our mutants were determined entirely independently from each other and from the wild-type enzyme. WAT451 observed in the wild-type structure was replaced by a sulfate ion, in both the mutants. While a second sulfate with half occupancy was located near the wild-type WAT478 in the C42A mutant, this position was occupied by WAT536 in the C42S mutant. The interactions of these sulfate ions with the enzyme and water molecules are given in Table 4. These sulfates are located near the N-terminal ends of short α-helices, allowing favorable interaction of the dianion charge with the α-helix dipole (Wada, 1976; Hol *et al.*, 1978; Chakrabarti, 1993).

Table 5: Interactions of the Guanidinium Group of Arg 303 in the C42A and C42S Mutants and Wild-Type NADH Peroxidase

	distances (Å) C42A	C42S	wild-type
Arg 303 N$^{\eta 1}$···His10N$^{\delta 1}$	3.1	3.2	3.0
···center Tyr60	3.8	3.8	3.7
Arg 303 N$^{\eta 2}$···Glu14 O$^{\epsilon 2}$	2.8	2.8	2.9
···WAT662[a]/WAT706[b]	3.1	3.3	
···WAT486[a]/WAT470[b]/WAT489[c]	2.7	2.8	2.7
Arg 303 N$^{\epsilon}$···Glu14 O$^{\epsilon 2}$	3.1	3.2	3.3

[a] In C42A mutant. [b] In C42S mutant. [c] In wild type.

Catalytic Mechanism of NADH Peroxidase. We have reported (Parsonage & Claiborne, 1995) the results of a detailed analysis of the kinetic and redox properties of the NADH peroxidase Cys42Ala and Cys42Ser mutants. Both mutants have turnover numbers approximately 0.04% that of the wild-type enzyme; in keeping with elimination of the Cys42-SOH redox center, each mutant is fully reduced with 1 equiv of NADH or dithionite per FAD in static titrations. Stopped-flow analysis has shown that, in each case, flavin reduction is rapid (k_{obs} = 300−500 s^{-1} at 5 °C), further demonstrating that the reduced Cys42-SH is required for H_2O_2 reduction in the wild-type enzyme. Surprisingly, the flavin redox potentials for the two mutants (−197 and −219 mV for Cys42Ala and Cys42Ser, respectively) are approximately 100 mV higher than that for the reduced Cys42-SH (EH_2) form of the wild-type peroxidase. This increase in redox potentials of the mutants might have been due to significant conformational change of the protein but the close structural similarity of wild-type and mutant enzymes rules out that possibility. Since the redox potentials of the two mutants are so similar, the available evidence supports the conclusion that the reduced redox potential of wild-type enzyme is due to the charge transfer interaction between oxidized FAD and the electron-rich Cys 42 thiolate in the EH_2 species.

In addition to Cys 42, another residue which is possibly involved in catalysis is His 10. In the reaction mechanism proposed by Stehle *et al.* (1993) it is assumed that the imidazole function of this residue shuttles between protonated and unprotonated states. In our mutant structures at 2.0 Å resolution the position of His 10 is virtually the same as in the 2.16 Å wild-type structure (Stehle *et al.*, 1991) of the NADH peroxidase with no atom deviating more than 0.3 Å. His 10 in all structures is close to the positively charged guanidinium group of Arg 303. Since the positive charge of this guanidinium function is likely to affect the proton affinity of His 10, first an analysis of the environment of Arg 303 is given and then the consequences for the properties of His 10 are discussed.

The interactions of Arg 303 in our mutant structures show interesting features which can be put in perspective of several recent studies on the environment of arginine side chains in protein structures (Nandi *et al.*, 1993; Borders *et al.*, 1994; Flocco & Mowbrey, 1994). The neighboring atoms of the guanidinium group of Arg 303 in both the C42A and C42S mutants are listed in Table 5 and depicted in Figure 4. The interactions of this residue can be described as follows:

(i) A salt bridge is formed with Glu 14. Both the N$^{\eta 2}$ and N$^{\epsilon}$ atoms of Arg 303 are engaged in hydrogen bonds with the carboxylate of Glu 14 (with guanidinium-to-

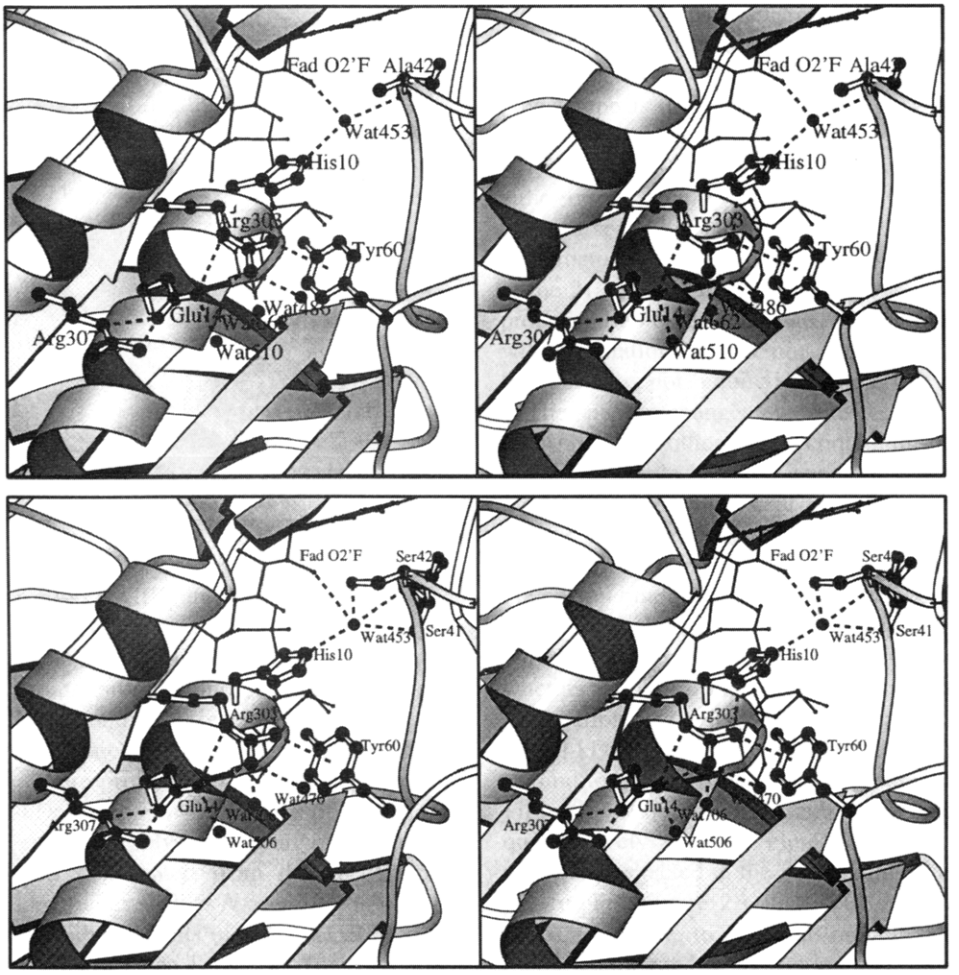

FIGURE 4: Stereoview of the environment of Arg303 drawn using MOLSCRIPT (Kraulis, 1991). Note the interaction of the guanidinium group with the phenyl ring of Tyr60 indicated by dotted line connecting $N^{\eta 1}$ and the center of the phenyl ring of Tyr 60 (see text for discussion). (a, top) The mutant C42A; (b, bottom) C42S.

carboxylate distances of 2.8 and 3.1 Å in C42A and 2.8 and 3.2 Å in C42S, respectively).

(ii) Two solvent molecules (WAT486 and WAT662 in C42A; WAT470 and WAT 706 in C42S) are at hydrogen bond distances from the $N^{\eta 2}$ atom. The angular hydrogen bond geometry is particularly good in C42A for WAT486 (and in C42S for WAT470) and is accompanied by a relatively short hydrogen bond distance.

(iii) The $N^{\eta 1}$ atom of Arg 303 is relatively close to the $N^{\delta 1}$ atom of the active site His 10. The interatomic distance is 3.1 Å in C42A and 3.2 Å in C42S with temperature factors of less than 15.0 $Å^2$ for both atoms. The angular geometry of the His 10 $N^{\delta 1}$ to Arg 303 $N^{\eta 1}$ hydrogen bond is reasonable as reflected in values of 122° for Arg 303 C^{ζ}−Arg 303 $N^{\eta 1}$−His 10 $N^{\delta 1}$ in both C42A and C42S mutants. The angle His 10 C^{γ}−His 10 $N^{\delta 1}$−Arg 303 $N^{\eta 1}$ is 144° in both mutants. These geometric values indicate that Arg 303 $N^{\eta 1}$ forms a hydrogen bond with $N^{\delta 1}$ of His10 and, consequently, that His10 is unprotonated.

(iv) The phenyl ring of Tyr 60 is located such that the center of the ring is 3.8 Å away from the $N^{\eta 1}$ atom of Arg 303 in both the mutants. The plane of the guanidinium group is approximately perpendicular to the plane of the phenyl ring. This geometry is indicative of a favorable interaction between the charge of the arginine and the π system of the phenyl ring, mediated by the hydrogen atom of $N^{\eta 1}$. The angle Tyr 60 C^{β}−center phenyl Tyr 60−Arg 303 $N^{\eta 1}$ is 94° in C42A and 90° in C42S, respectively, while the angle Arg 303 C^{ζ}−Arg 303 $N^{\eta 1}$−center phenyl Tyr 60 is 144° in C42A and 147° in C42S. These angles show that the $N^{\eta 1}H$ group of the arginine ring points to the π system of the side chain of Tyr 60. This arrangement of the guanidinium group of Arg 303 with respect to Tyr 60 is another example of hydrogen bonds involving phenyl rings in proteins as described by Flocco and Mowbray (1994).

The quite interesting environment of Arg 303 is very similar in our mutant structures and in the wild-type enzyme. The phenyl ring of Tyr 60 deviates by less than 0.3 Å; the carboxylate of Glu 14 superimposes within 0.2 Å in all three structures. Most importantly the interaction of His 10 and Arg 303 is very similar in wild-type and mutant enzymes. Hence, it is very likely that also in wild-type enzyme His 10 is unprotonated throughout the catalytic cycle requiring some modifications of the detailed catalytic mechanism. The role of residues His 10, Arg 303, and Tyr 60 is currently subject of further mutagenesis and enzymological investigations and results will be reported in the future.

CONCLUSIONS

We have shown unequivocally that the NADH peroxidase mutants C42A and C42S have a three-dimensional structure which is virtually indistinguishable from that of the wild-type enzyme. This shows that removal of the sulfhydryl group of Cys 42 is responsible for the drop in activity by a

factor of approximately 2500 when comparing wild-type with the two mutant enzymes investigated.

ACKNOWLEDGMENT

We would like to thank Stewart Turley for help in data collection, Christophe Verlinde and Vivien Yee for assistance with computational problems, and Shekhar Mande for stimulating discussions. We also thank the CHESS synchrotron and staff for access to the powerful X-ray beam and assistance in obtaining excellent data.

REFERENCES

Benen, J., van Berkel, W., Zak, Z., Visser, T., Veeger, C., & de Kok, A. (1991) *Eur. J. Biochem. 202*, 863−872.

Borders, C. L., Jr., Broadwater, J. A., Bekeny, P. A., Salmon, J. E., Lee, A. S., Eldridge, A. M., & Pett, V. B. (1994) *Protein Sci. 3*, 541−548.

Brünger, A. T., Kuriyan, J., & Karplus, M. (1987) *Science 235*, 458−460.

CCP4, Collaborative Computational Project, No. 4 (1994) *Acta Crystallogr. D50*, 760−763.

Chakrabarti, P. (1993) *J. Mol. Biol. 234*, 463−482.

Claiborne, A., Ross, R. P., & Parsonage, D. (1992) *Trends Biochem. Sci. 17*, 183−186.

Claiborne, A., Miller, H., Parsonage, D., & Ross, R. P. (1993) *FASEB J. 7*, 1483− 1990.

Claiborne, A., Ross, R. P., Ward, D., Parsonage, D., & Crane, E. J., III (1994) in *Flavins and Flavoproteins 1993* (Yagi, K., Ed.) pp 587−596, Walter de Gruyter & Co., New York.

Connolly, M. L. (1983) *J. Appl. Crystallogr. 16*, 548−558.

Epp, O., Ladenstein, R., & Wendel, A. (1983) *Eur. J. Biochem. 133*, 51−69.

Flocco, M. M., & Mowbray, S. L. (1994) *J. Mol. Biol. 235*, 709−717.

Flohé, L., Loschen, G., Günzler, W. A., & Eichele, E. (1972). *Hoppe-Seyler's Z. Physiol. Chem. 353*, 987−999.

Hall, S. R., & Stewart J. M. (1987) *Editors of XTAL2.2 User's Manual*, Universities of Western Australia and Maryland.

Hol, W. G. J., van Duijnen, P. T., & Berendsen, H. J. C. (1978) *Nature 273*, 443−446.

Howard, A. J., Gilliland G. L., Finzel, B. C., Poulos, T. L., Ohlendorf, D. M., & Salemme, F. R. (1987) *J. Appl. Crystallogr. 20*, 383−387.

Jones, T. A., Zou, J. Y., & Cowan, S. W. (1991) *Acta Crystallogr. 47*, 110−119.

Kamphuis, I. G., Kalk, K. H., Swarte, M. B. A., & Drenth, J. (1984) *J. Mol. Biol. 179*, 233− 256.

Karplus, P. A., & Schulz, G. E. (1987) *J. Mol. Biol. 195*, 701−729.

Kraulis, P. J. (1991) *J. Appl. Crystallogr. 24*, 946−950.

Laskowski, R. A., MacArthur, N. W., Moss, D. S., & Thornton, J. M. (1993). *J. Appl. Crystallogr. 26*, 283−290.

Leslie, A. G. W., Brick, P., & Wonacott, A. T. (1986) MOSFLM, *Inf. Quart. Protein Crystallogr. 18*, 33−39.

Mattevi, A., Obmolova, G., Sokatch, J. R., Betzel, C., & Hol., W. G. J. (1992) *Proteins: Struct., Funct., Genet. 13*, 336−351.

Mattevi, A., Obmolova, G., Kalk, K. H., van Berkel, J. H., & Hol., W. G. J. (1993) *J. Mol. Biol. 230*, 1200−1215.

Nandi, C. L., Singh, J., & Thornton, J. M. (1993) *Protein Eng. 6*, 247−259.

Parsonage, D., & Claiborne, A. (1995) *Biochemistry 34*, 435−441.

Pathak, D., Ashley, G., & Ollis, D. (1991) *Proteins: Struct., Funct., Genet. 9*, 267−279.

Poole, L. B., & Claiborne, A. (1989a) *J. Biol. Chem. 264*, 12330−12338.

Poole, L. B., & Claiborne, A. (1989b) *J. Biol. Chem. 264*, 12322−12329.

Ramachandran, G. N., & Sasisekharan, V. (1968) *Adv. Protein Chem. 23*, 283−438.

Read, R. J. (1986) *Acta Crystallogr. A42*, 140−149.

Rietveld, P., Arscott, L. D., Berry, A., Scrutton, N. S., Deonarain, M. P., Perham, R. N., & Williams, C. H., Jr. (1994) *Biochemistry 33*, 13888−13895.

Ross, R. P., & Claiborne, A. (1991) *J. Mol. Biol. 221*, 857−871.

Stehle, T., Ahmed, S. A., Claiborne, A., & Schulz, G. E. (1991) *J. Mol. Biol. 221*, 1325− 1344.

Stehle, T., Claiborne, A., & Schulz, G. E. (1993). *Eur. J. Biochem. 211*, 221−226.

Wada, A. (1976) *Adv. Biophys. 9*, 1−63.

Williams, C. H., Jr. (1992) in *Chemistry and Biochemistry of Flavoenzymes* (Müller, F., Ed.) Vol. III, pp 121−211, CRC Press, Boca Raton, Florida.

BI950056J